5G Vehicle Positioning in Tunnels with Single Anchor TDOA Exploiting Multipath Reflectors

Lorenzo Italiano, Mattia Brambilla, Monica Nicoli
Politecnico di Milano, Milan, Italy

***Abstract*—We investigate the problem of vehicle positioning inside a tunnel, addressed by exploiting 5G cellular uplink signals received by a single anchor station, e.g., a base station (BS) or road-side unit (RSU). Leveraging the multipath component (MPC) characterization introduced in 3GPP Release 17, which labels each signal arrival as line-of-sight (LOS) or non-line-of-sight (NLOS), we exploit the MPC identification of received signal echoes to enhance vehicle positioning. Assuming the availability of high-definition maps of the environment, we embed their knowledge with MPC data to dynamically identify signal reflectors and convert the environment into a network of auxiliary anchors for positioning. The proposed framework leverages single-anchor time difference of arrival (SA-TDOA) alongside angle of arrival (AOA) measurements. In contrast to standard TDOA approaches, the SA-TDOA measurement does not require synchronization between the mobile terminal and the anchor, nor the synchronization among the anchors, thus favoring its adoption in real-world deployments. A joint tracking of the vehicle and reflectors is performed by means of an extended Kalman filter. Simulation results demonstrate the augmentation capability of the proposed method, which exhibits high accuracy and robustness in both LOS and NLOS scenarios.**

***Index Terms*—5G positioning, 3GPP Rel-17, multipath, reflectors, SA-TDOA, ZF-MUSIC.**

I. Introduction

High-accuracy positioning in confined environments, such as indoor spaces or tunnels, is severely affected by non-line-of-sight (NLOS) conditions and multipath propagation [1]. Traditional algorithms relying on a geometry-based modeling assuming line-of-sight (LOS) are often degraded by these effects, as they do not fully exploit the valuable information inherently present in multipath signals. With the advent of fifth-generation (5G) technology, a paradigm shift in positioning is emerging, thanks to the capability of resolving early multipath components (MPCs). This unlocks new opportunities for highly accurate positioning, even in challenging scenarios such as connected automated driving [2]. In this context, our study addresses a vehicular tunnel scenario, as illustrated in Fig. 1.

Recently, new techniques have been emerging to convert multipath into auxiliary information for positioning. In [3], the authors exploit a pseudo maximum likelihood for direct positioning estimation to address dynamic multipath environments. In [4], a weighted least squares approach is applied for tri-dimensional (3D) positioning using angle of arrival (AOA) and time of arrival (TOA) measurements, leveraging virtual base stations (BSs) inferred from a geometric map. The authors in [5] demonstrate the feasibility of single-anchor

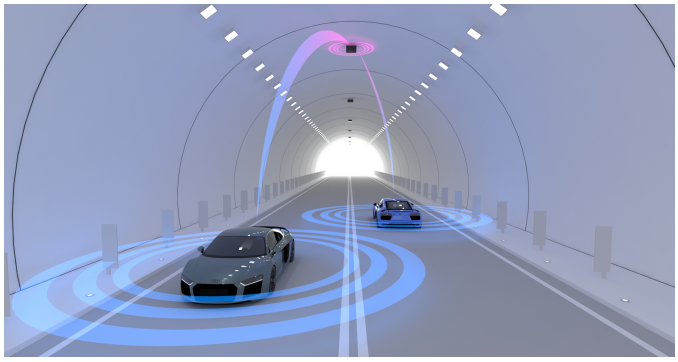

Fig. 1. Tunnel localization scenario with two connected vehicles exploiting a 5G BSs for positioning.

time difference of arrival (SA-TDOA), a synchronization-free measurement, by conducting both simulations and field tests, leveraging a floor plan of the reflecting surfaces (called reflectors) to operate in NLOS scenarios. Their proposal relies on a two-step estimate of reflectors and user equipment (UE) locations. A field test with mmWave 5G is presented in [6], integrating simultaneous localization and mapping (SLAM) and device synchronization in a single BS vehicular scenario using round-trip time (RTT) with AOA and angle of departure (AOD) measurements. However, SA-TDOA was not considered, and RTT is unsuitable for high-speed scenarios because of latency constraints. Additionally, several studies have explored the use of reflective intelligent surfaces (RISs) to enhance the estimation of virtual anchors [7].

State-of-the-art approaches favor the estimate of virtual anchors over reflectors due to their fixed positions [8], but their simplistic assumptions limit real-world applicability. Virtual anchor estimation is based on the method of images used in electromagnetics to simplify the analysis of wave reflections [9]. Literature studies assume plane walls with perfect reflections, reducing virtual anchor estimation to a mirror image problem. Realistic scenarios present irregular or curved surfaces, so the computation of the virtual anchors becomes challenging and requires case-specific models, limiting the generalization of the methodology. To overcome this issue, we propose to estimate the reflectors as an alternative to virtual anchors. Different from recent works performing joint reflector and device localization using TOA and AOA measurements with perfect synchronization [10], our approach better reflects real-world conditions with asynchronous networks and avoids the impractical need for large antenna arrays at both sides as in other single-bounce reflection (SBR) methods [11], [12].

In this work, we propose a positioning methodology framed in the 3rd Generation Partnership Project (3GPP) Release 17 to accurately estimate the position of a vehicle traveling through a tunnel. While 3GPP Release 16 introduced dedicated positioning signals, designed to provide sharp cross-correlation peaks for precise MPC identification [13], 3GPP Release 17 has enhanced the MPC characterization by labeling each signal arrival as LOS or NLOS [14]. Moreover, future BSs and roadside units (RSUs) are expected to access high-definition (HD) maps [15] generated through 5G SLAM or LiDAR systems [16]. By combining HD maps with MPC data, reflectors can be dynamically identified, converting the environment into a network of auxiliary positioning anchors.

The proposed framework leverages a single BS mounted in the tunnel, measuring AOA and TDOA of multiple arriving signals from a transmitting on-board unit (OBU) to localize the vehicle. We broadly refer to the localizing device at the roadside as an anchor, as it can be considered both as a BS and an RSU using the sidelink. The proposed method exploits SA-TDOA and AOA measurements, the latter are estimated through a sequential zero-forcing (ZF) multiple signal classification (MUSIC) algorithm. An extended Kalman filter (EKF) is then employed to jointly track the positions of the reflectors and the vehicular UE. This approach exhibits strong performance and robustness in both LOS and NLOS scenarios without relying on synchronization, proving to be a reliable solution for tunnels and other global navigation satellite systems (GNSS)-denied environments.

The paper is structured as follows: Sec. II presents the system and measurement models; Sec. III describes the proposed methodology; Sec. IV illustrates the simulations and discusses the results; Sec. V concludes the work.

II. Positioning Model and Measurements

A. Wireless Channel Model

We consider a time-slotted uplink (UL) single-input multiple-output (SIMO) orthogonal frequency-division multiplexing (OFDM) wireless link. The transmit vehicle has a single antenna, while the receiving anchor has an array of $N_{\mathrm{rx}} = M \times N$ antenna elements. The matrix $\mathbf{H}_\tau \in \mathbb{C}^{N_{\mathrm{rx}} \times 1}$ represents the τ-th tap of the channel response. The received signal at discrete time $t = 1, 2, \ldots, T$ (sampled at symbol time T_s), is modeled as:

$$\mathbf{y}_t = \sum_{\tau=0}^{T_{\mathrm{cp}}-1} \mathbf{H}_\tau \, s_{t-\tau} + \mathbf{n}_t \quad \in \mathbb{C}^{N_{\mathrm{rx}} \times 1}, \tag{1}$$

where $s_t \in \mathbb{C}$ is the transmitted signal at time t and $\mathbf{n}_t \in \mathbb{C}^{N_{\mathrm{rx}} \times 1}$ is the noise. The SIMO channel is modeled as a combination of P correlated paths as:

$$\mathbf{H}_\tau = \sum_{p=1}^{P} \alpha_p \, \mathbf{a}_{\mathrm{rx}}(\boldsymbol{\theta}_{\mathrm{rx},p}) \, \mathrm{g}(\tau - \tau_p), \tag{2}$$

where each path p may be closely spatially clustered with other paths and it is characterized by a complex fading amplitude α_p, the receiving antenna array response $\mathbf{a}_{\mathrm{rx}}(\cdot) \in \mathbb{C}^{N_{\mathrm{rx}} \times 1}$ to AOAs $\boldsymbol{\theta}_{\mathrm{rx},p} = \left[\phi_{\mathrm{rx},p} \, \psi_{\mathrm{rx},p}\right]^\top$, composed by the azimuth $\phi_{\mathrm{rx},p}$ and the elevation $\psi_{\mathrm{rx},p}$, and the pulse waveform $\mathrm{g}(\cdot)$ delayed by the path delay τ_p, with $\max_p(\tau_p) \leq T_{\mathrm{cp}}$. We assume a block-fading channel response, with maximum path delay contained within the cyclic prefix T_{cp}, and with path delays and AOAs constant within an OFDM symbol [2].

B. AOA Measurements

To estimate the AOAs from (2) and their uncertainties, we consider the sequential ZF-MUSIC algorithm, a super-resolution techniques for AOA estimation based on MUSIC [17]. Let $\mathbf{R} = \mathrm{E}\left[\mathbf{y}_t \, \mathbf{y}_t^{\mathrm{H}}\right] \simeq \frac{1}{T} \sum_{t=1}^{T} \mathbf{y}_t \, \mathbf{y}_t^{\mathrm{H}}$ denote the covariance of $\mathbf{y}_t$, with $\mathrm{E}[\cdot]$ the expected value and $(\cdot)^{\mathrm{H}}$ the hermitian operator. Consider its eigenvalue decomposition $\mathbf{R} = \mathbf{U}_{\mathrm{s}} \Lambda_{\mathrm{s}} \mathbf{U}_{\mathrm{s}} + \mathbf{U}_{\mathrm{n}} \Lambda_{\mathrm{n}} \mathbf{U}_{\mathrm{n}}$ to extract the signal and the noise subspace eigenvectors, $\mathbf{U}_{\mathrm{s}}$ and $\mathbf{U}_{\mathrm{n}}$, containing respectively the eigenvector corresponding to the P largest and the $N_{\mathrm{rx}} - P$ smallest eigenvalues in $\boldsymbol{\Lambda}_{\mathrm{s}}$ and $\boldsymbol{\Lambda}_{\mathrm{n}}$. The MUSIC pseudo-spectrum is given by:

$$\mathbf{PS}_{\mathrm{MUSIC}}(\boldsymbol{\theta}) = \frac{1}{\mathbf{a}_{\mathrm{rx}}^{\mathrm{H}}(\boldsymbol{\theta}) \, \mathbf{U}_{\mathrm{n}} \, \mathbf{U}_{\mathrm{n}}^{\mathrm{H}} \, \mathbf{a}_{\mathrm{rx}}(\boldsymbol{\theta})}, \tag{3}$$

where the steering vector $\mathbf{a}_{\mathrm{rx}}(\boldsymbol{\theta})$ spans over a set of angles, detecting the directions with the highest signal intensity.

Since the P signal MPCs are correlated, to compensate for the MUSIC degraded performances, bi-dimensional (2D) forward-backward spatial smoothing is employed as in [18]. Spatial smoothing takes advantage of the translation properties of a uniform array by dividing the full array into $M_s N_s$ overlapping sub-arrays of dimension $M_1 \times N_1$, where $M_1 = M - M_s + 1$ and $N_1 = N - N_s + 1$. Indicating the received signal at (m, n)-th sub-array as $\mathbf{y}_t^{(m,n)}$ and its covariance as $\mathbf{R}_{mn}$, we define the spatial smoothing covariance matrix as:

$$\mathbf{R}^{\mathrm{f}} = \frac{1}{M_s N_s} \sum_{m=1}^{M_s} \sum_{n=1}^{N_s} \mathbf{R}_{mn}, \tag{4}$$

and its forward-backward version as:

$$\mathbf{R}^{\mathrm{fb}} = \frac{1}{2} \left[\mathbf{R}^{\mathrm{f}} + \boldsymbol{\Omega} \, (\mathbf{R}^{\mathrm{f}})^* \, \boldsymbol{\Omega}\right], \tag{5}$$

where $(\cdot)^*$ is the complex conjugate, and $\boldsymbol{\Omega}$ is a matrix of appropriate dimension with ones in its anti-diagonal and zeros elsewhere.

MUSIC accuracy can be enhanced by sequentially removing previously estimated AOAs using the ZF method as in [19]. Recalling (3), the ZF-MUSIC pseudo-spectrum of the path p is computed as:

$$\mathbf{PS}_{\mathrm{ZF-MUSIC}}^{(p)}(\boldsymbol{\theta}) = \mathcal{F}_p(\boldsymbol{\theta}) \; \mathbf{PS}_{\mathrm{MUSIC}}(\boldsymbol{\theta}), \tag{6}$$

where $\mathcal{F}_p(\cdot)$ is the ZF function defined as $\mathcal{F}_p(\boldsymbol{\theta}) = N_{\mathrm{rx}}^{-1} \mathbf{a}_{\mathrm{rx}}^{\mathrm{H}}(\boldsymbol{\theta}) \mathbf{V}_p^{\perp} \, \mathbf{a}_{\mathrm{rx}}(\boldsymbol{\theta})$, and $\mathbf{V}_p^{\perp} = \mathbf{I} - \mathbf{V}_p$ is the orthogonal projector onto the space spanned by the previously $p-1$ estimated AOAs, in which

$$\mathbf{V}_p = \begin{cases} \mathbf{I} & \text{if } p = 1, \\ \mathbf{A}_p \left(\mathbf{A}_p^{\mathrm{H}} \mathbf{A}_p\right)^{-1} \mathbf{A}_p^{\mathrm{H}} & \text{otherwise,} \end{cases} \tag{7}$$

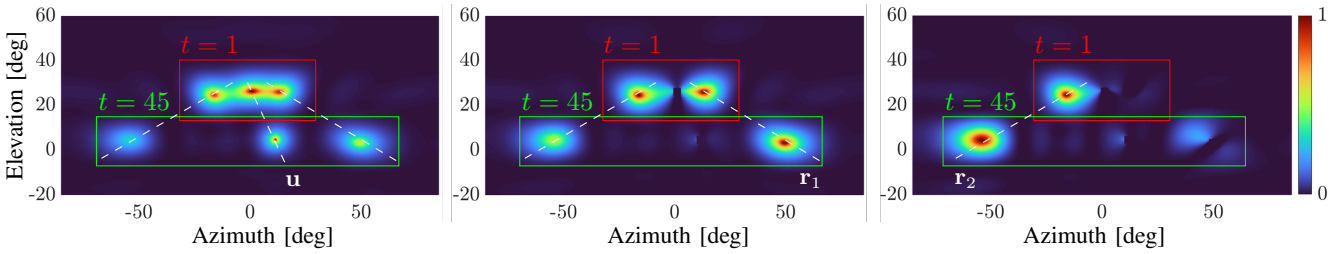

Fig. 2. ZF-MUSIC spectra over three algorithm iterations, with each spectrum displaying results for time $t = 1$ (red box) and $t = 45$ (green box). The peaks in the middle correspond to the UE, while those on the sides to the reflectors. Each track is indicated with a dashed white line.

and $\mathbf{A}_p = N_{\text{rx}}^{-0.5}\left[\mathbf{a}_{\text{rx}}(\widehat{\boldsymbol{\theta}}_{\text{rx},1}) \cdots \mathbf{a}_{\text{rx}}(\widehat{\boldsymbol{\theta}}_{\text{rx},p-1})\right]$. As a last step, we iteratively estimate the p-th AOA and its associated covariance exploiting the pseudo-spectrum nature. The estimated AOA for the p-th path is $\widehat{\boldsymbol{\theta}}_{\text{rx},p} = \arg\max_{\boldsymbol{\theta}} \{\mathbf{PS}^{(p)}_{\text{ZF-MUSIC}}(\boldsymbol{\theta})\}$, while the covariance is obtained by normalizing the pseudo-spectrum and identifying the ellipse corresponding to the 60% contour level. The confidence ellipse is then used to compute the covariance of the AOA measurement. Fig. 2 illustrates the ZF-MUSIC spectrum of two different time instants over the algorithm iterations.

C. SA-TDOA Measurements

Assuming UL measurements, let t_{rx} and t_{tx} be the receive and transmit time at the anchor and UE, respectively. The measured TOA of the p-th at the anchor is:

$$\tau_p = t_{\text{rx},p} - t_{\text{tx},p} + \delta = \frac{d_p}{c} + \delta, \tag{8}$$

where δ is the clock offset between UE and the anchor, d_p is the p-th path distance, and c the speed of light. The TOA is assumed to be known with an accuracy that is inversely proportional with respect to the signal bandwidth. To compensate for the UE-anchor clock offset, a common methodology is to compute the TDOA of the same transmitted signal at two anchors. However, this approach does not solve the clock offset between the anchors.

To deal with non-synchronous BSs, we consider the so-called SA-TDOA as the difference between the TOAs of the different MPCs for a single anchor. Given two generic paths $p \in \{1, 2\}$ of the same signal received at an anchor located at the 3D position $\mathbf{s}$, the SA-TDOA is defined as:

$$\Delta\tau_{1,2} = \tau_1 - \tau_2 = \frac{d_1 - d_2}{c}. \tag{9}$$

Both paths can have zero or multiple reflections; however, in this work, we consider a maximum of two paths with one reflection per path. Therefore, the path distance for a MPC is given by $d_p = \|\mathbf{r}_p - \mathbf{u}\| + \|\mathbf{s} - \mathbf{r}_p\|$, with $\mathbf{r}_p$ the location of the reflector for path p and $\|\cdot\|$ the Euclidean norm. The proposed SA-TDOA approach is suited for those contexts where synchronization among the network nodes cannot be guaranteed with the precision required by positioning applications. As an example, it could be exploited in cellular networks, which are characterized by relaxed constraints on inter-BSs synchronization [20], [21].

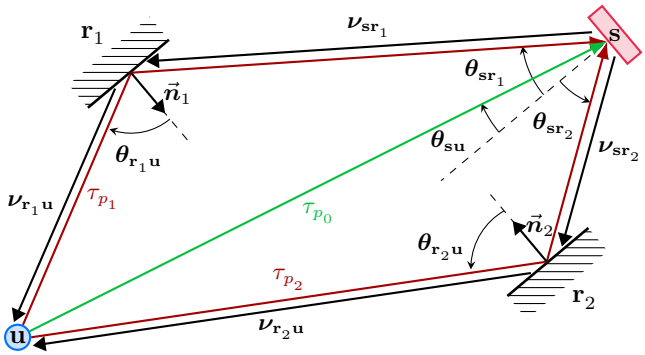

Fig. 3. Geometrical representation of the localization problem involving UE $\mathbf{u}$ (blue circle), anchor $\mathbf{s}$ (red rectangle), reflectors $\mathbf{r}_1$ and $\mathbf{r}_2$ (on the walls), and the associated vectors and measurements, all reference to their local coordinate system.

III. Proposed Localization Methodology

We propose to obtain the vehicle localization by estimating and tracking the joint state $\mathbf{x} = [\mathbf{u}\,\mathbf{r}_1\,\mathbf{r}_2]^\top$, including the 3D coordinates of the UE $\mathbf{u}$ and the reflectors $\mathbf{r}_1$ and $\mathbf{r}_2$, with $\mathbf{r}_p \in \mathcal{P}_p$, with $\mathcal{P}_p$ representing the plane of the signal reflector, assumed to be known from the knowledge of the HD map. The estimated variables are time-dependent, but in this section, we omit the dependency on subscript t for an easier formulation. A schematic overview of the problem with the associated measurements is reported in Fig. 3, and detailed in the following.

The path in LOS between the UE and the anchor provides the AOA $\boldsymbol{\theta}_{\mathbf{su}} = [\phi_{\mathbf{su}}\ \psi_{\mathbf{su}}]^\top$. Additionally, the combination of LOS and MPCs enables the estimation of two SA-TDOAs measurements: $\Delta\tau_{\mathbf{sr}_1\mathbf{u}} = \tau_{\mathbf{sr}_1} - \tau_{\mathbf{su}}$ and $\Delta\tau_{\mathbf{sr}_2\mathbf{u}} = \tau_{\mathbf{sr}_2} - \tau_{\mathbf{su}}$. Furthermore, the MPCs alone provide: an additional SA-TDOA between the two reflected paths $\Delta\tau_{\mathbf{sr}_1\mathbf{r}_2} = \tau_{\mathbf{sr}_1} - \tau_{\mathbf{sr}_2}$, the AOAs $\boldsymbol{\theta}_{\mathbf{sr}_p} = \left[\phi_{\mathbf{sr}_p}\ \psi_{\mathbf{sr}_p}\right]^\top$ between the anchor $\mathbf{s}$ and the reflector $\mathbf{r}_p$, and the distances given by the intersection of the planes $\mathcal{P}_p$ and the vectors $\boldsymbol{\nu}_{\mathbf{sr}_p} = \left[\cos\phi_{\mathbf{sr}_p}\cos\psi_{\mathbf{sr}_p}\quad \sin\phi_{\mathbf{sr}_p}\cos\psi_{\mathbf{sr}_p}\quad \sin\psi_{\mathbf{sr}_p}\right]^\top$. Given the tunnel planimetry knowledge, we can also compute the angles $\boldsymbol{\theta}_{\mathbf{r}_p\mathbf{u}}$ between the reflectors $\mathbf{r}_p$ and the UE $\mathbf{u}$ from the reflection $\boldsymbol{\nu}_{\mathbf{r}_p\mathbf{u}} = \boldsymbol{\nu}_{\mathbf{sr}_p} - 2\left(\boldsymbol{\nu}_{\mathbf{sr}_p}^\top \vec{\boldsymbol{n}}_p\right)\vec{\boldsymbol{n}}_p$ of the signal on the

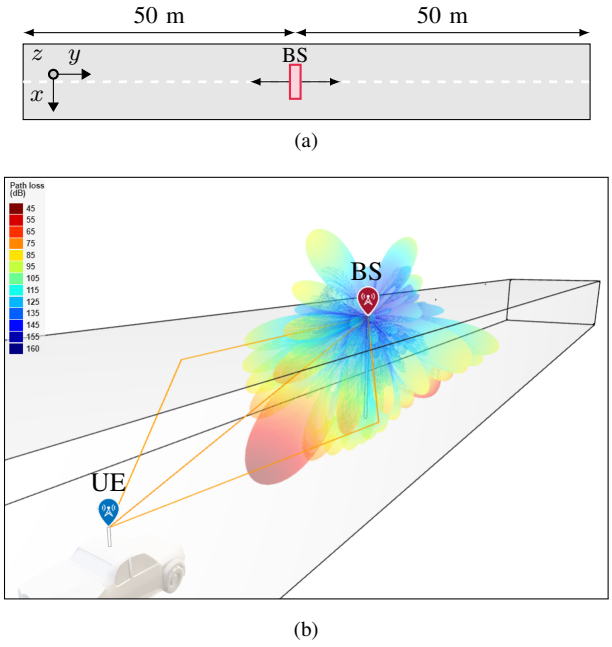

Fig. 4. Implemented tunnel scenario. (a) Top view. (b) 3D representation in *MATLAB Site Viewer* with a raytracer example. The red marker denotes a BS, while the blue marker is for the vehicle. Beamforming gains at broadside and multipath propagation are represented as well.

TABLE I
SUMMARY OF UE POSITIONING PERFORMANCE METRICS

	SA-JURE 5G LOS	SA-JURE 5G NLOS	TOA+AOA 5G LOS	SA-JURE C-V2X LOS
2D RMSE [m]	0.69	1.18	2.37	1.38
2D MAE [m]	0.57	1.00	1.93	1.14
X-MAE [m]	0.10	0.26	0.37	0.41

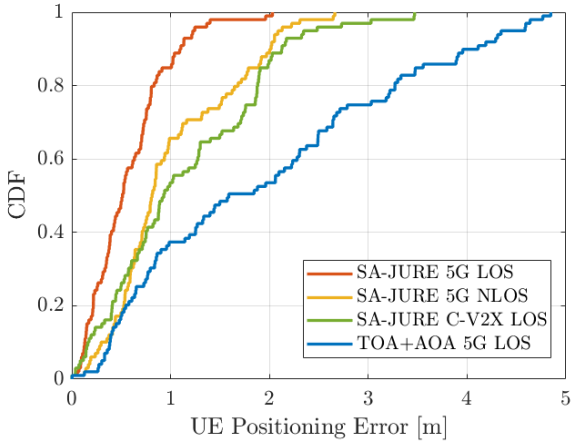

Fig. 5. CDF of the 2D positioning error of the experiments.

tunnel wall, as:

$$\boldsymbol{\theta}_{\mathbf{r}_p\mathbf{u}} = \left[\operatorname{atan}\left(\nu_{y,\mathbf{r}_p\mathbf{u}}, \nu_{x,\mathbf{r}_p\mathbf{u}}\right) \quad \arcsin\frac{\nu_{z,\mathbf{r}_p\mathbf{u}}}{\|\boldsymbol{\nu}_{\mathbf{r}_p\mathbf{u}}\|}\right]^\top, \quad (10)$$

where $\vec{\boldsymbol{n}}_p$ is the plane $\mathcal{P}_p$ norm vector.

The estimation methodology for $\mathbf{x}$ follows the EKF approach, where we distinguish between the measurements in LOS and NLOS. The measurement model $\mathbf{h}(\mathbf{x})$ can be computed in closed form for both visibility conditions according to the geometrical relationships previously specified, which leads to the following definition:

$$\mathbf{h}(\mathbf{x}) = \begin{cases} \left[\boldsymbol{\theta}_{\mathbf{su}}^\top \tau_{\mathbf{sr}_1} \boldsymbol{\theta}_{\mathbf{r}_1\mathbf{u}}^\top \tau_{\mathbf{sr}_2} \boldsymbol{\theta}_{\mathbf{r}_2\mathbf{u}}^\top \Delta\tau_{\mathbf{sr}_1\mathbf{u}} \Delta\tau_{\mathbf{sr}_2\mathbf{u}}\right]^\top & \text{if LOS,} \\ \left[\boldsymbol{\theta}_{\mathbf{sr}_1}^\top \tau_{\mathbf{sr}_1} \boldsymbol{\theta}_{\mathbf{sr}_2}^\top \tau_{\mathbf{sr}_2} \boldsymbol{\theta}_{\mathbf{r}_1\mathbf{u}}^\top \boldsymbol{\theta}_{\mathbf{r}_2\mathbf{u}}^\top \Delta\tau_{\mathbf{sr}_1\mathbf{r}_2}\right]^\top & \text{if NLOS.} \end{cases}$$

The EKF state model assumes a random walk model for $\mathbf{r}_1$ and $\mathbf{r}_2$ and a velocity sensor model for $\mathbf{u}$ [22].

IV. Simulations and Results

To validate our framework, we consider a vehicular tunnel environment, modeled as a cuboid of dimensions $10\,\mathrm{m} \times 100\,\mathrm{m} \times 5\,\mathrm{m}$. A single anchor is placed in the middle of the tunnel at a height of $4.8\,\mathrm{m}$. It has two 10×10 antenna arrays pointing at opposite directions, as indicated in Fig. 4a, namely $(-90, -30)$ deg and $(90, -30)$ deg.

The tunnel environment is imported in *MATLAB* with *Site Viewer*, as shown in Fig. 4b, where the 5G UL sounding reference signal (SRS) is simulated using the *5G Toolbox* and a raytracer, allowing the extraction of AOAs and TOAs. The simulated 5G physical layer has carrier frequency $f_c = 3.8\,\mathrm{GHz}$, signal bandwidth of $100\,\mathrm{MHz}$, and transmit power of $23\,\mathrm{dBm}$. We assume that the first position (in the open air), the vehicle velocity along the tunnel, and the height of the vehicle are available at the BS side, which is a realistic assumption in a cooperative intelligent transport system (C-ITS) context leveraging cooperative awareness message (CAM) [23]. We also assume that the positions of reflectors along the transversal direction with respect to the road (x axis in Fig. 4a) are known from the knowledge of tunnel planimetry.

Our assessment considers the comparison of the proposed methodology, which we refer to as single-anchor joint UE and reflector estimation (SA-JURE), implemented both in LOS and NLOS-only conditions, with an UL-TOA+AOA single BS positioning approach without multipath augmentation (note that this approach is not applicable to NLOS condition). Both methodologies are applied to the 5G parametrization of the previous paragraph. This comparison allows the analysis of the performance degradation given by the BS-UE clock offset δ, modeled as a truncated Gaussian distribution with variance $50\,\mathrm{ns}$ and support $[-100, 100]\,\mathrm{ns}$ [21]. We also evaluate our SA-JURE for the current cellular vehicle-to-everything (C-V2X) standard in LOS, with carrier frequency at $5.9\,\mathrm{GHz}$ and $20\,\mathrm{MHz}$ bandwidth. The considered performance metrics on UE positioning include the 2D root mean square error (RMSE), the 2D mean absolute error (MAE), and the MAE along the x-axis (X-MAE), which is particularly relevant for lane detection. Their values are summarized in Table I, while Fig. 5 represents their cumulative density functions (CDFs).

Concerning the comparison of SA-JURE in LOS and NLOS, we observe that the system demonstrates high robustness to the loss of direct path information, with a degradation of approximately $0.5\,\mathrm{m}$ in RMSE and MAE, and $15\,\mathrm{cm}$ in X-

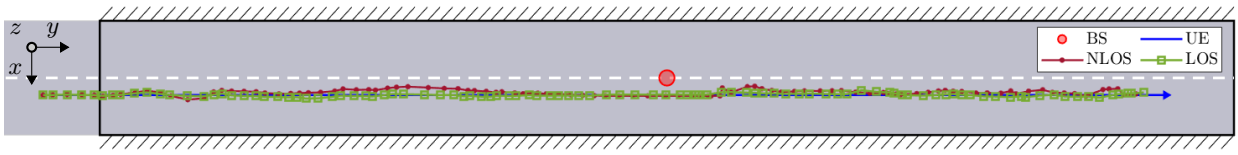

Fig. 6. Estimated vehicle trajectories by SA-JURE in LOS (green squares) and NLOS (dark red circles). The true trajectory is indicated with the blue line.

MAE. Moreover, we remark a very low X-MAE both in LOS and NLOS, ensuring a good accuracy for lane detection, which highly benefits from the knowledge of tunnel walls. Fig. 6 illustrates the performance of the proposed SA-JURE in both scenarios. Notice that when the vehicle is right under the BS, the lack of sufficient measurements prevents accurate position estimation. Therefore, in this region, the position is updated solely based on the motion model. The improvement of SA-JURE over a traditional single BS UL-TOA+AOA approach is remarkable, with an RMSE gain of 70%. Lastly, the assessment of SA-JURE implementation according to the current C-V2X standard with 20 MHz bandwidth demonstrates that the proposed method maintains good localization accuracy despite the small bandwidth, proving its reliability in positioning and highlighting its potential applicability.

V. Conclusion and Future Directions

In this work, we propose a positioning methodology that jointly estimates the position of a UE and the reflectors of the environment, converting them into auxiliary assistance data. The approach considers a single BS not affected by synchronization issues as it uses SA-TDOA and AOA measurements, together with map knowledge and MPC labeling introduced since 3GPP Release 17. Our findings demonstrate that it is possible to achieve highly accurate positioning inside a tunnel exploiting 5G signals in both LOS and NLOS scenarios and also using the C-V2X technology with spectrum confined to 20 MHz. Future works can consider the extension of the methodology assessment to more complex scenarios with irregular environmental planimetry, accounting for multiple reflections, adding random clutters, and jointly estimating angle and delay. These improvements will allow to assess the robustness of our approach under more challenging conditions similar to real-world tunnel environments.

Acknowledgment

This work was funded by the Italian Ministry of University and Research (MUR) Decree n. 352—09/04/2022 under the National Recovery and Resilience Plan (NRRP) and European Union (EU) NextGenerationEU project and by Autostrade per l'Italia (ASPI).

References

[1] H. Wymeersch, J. Lien, and M. Z. Win, "Cooperative localization in wireless networks," *Proc. IEEE*, vol. 97, no. 2, pp. 427–450, 2009.

[2] L. Italiano *et al.*, "A tutorial on 5G positioning," *IEEE Commun. Surveys Tuts.*, vol. 27, no. 3, pp. 1488–1535, 2025.

[3] A. Fascista, A. Coluccia, and G. Ricci, "A pseudo maximum likelihood approach to position estimation in dynamic multipath environments," *Signal Process.*, vol. 181, p. 107907, 2021.

[4] J. Liang, J. He, W. Yu, and T.-K. Truong, "Single-site 3-D positioning in multipath environments using DOA-delay measurements," *IEEE Wireless Commun. Lett.*, vol. 25, no. 8, pp. 2559–2563, 2021.

[5] M. R. Shamsian, M. Sadeghi, and F. Behnia, "Joint TDOA and DOA single site localization in NLOS environment using virtual stations," *IEEE Trans. Instrum. Meas.*, vol. 73, pp. 1–10, 2024.

[6] Y. Ge *et al.*, "Experimental validation of single BS 5G mmWave positioning and mapping for intelligent transport," *IEEE Trans. Veh. Technol.*, vol. 73, no. 11, pp. 16 744–16 757, 2024.

[7] Y. Zhu, B. Mao, and N. Kato, "On a novel high accuracy positioning with intelligent reflecting surface and unscented Kalman filter for intelligent transportation systems in B5G," *IEEE J. Sel. Areas Commun.*, vol. 42, no. 1, pp. 68–77, 2024.

[8] E. Leitinger *et al.*, "Evaluation of position-related information in multipath components for indoor positioning," *IEEE J. Sel. Areas Commun.*, vol. 33, no. 11, pp. 2313–2328, 2015.

[9] A. Zangwill, *Modern Electrodynamics*. Cambridge University Press, 2012, ch. 8.3, pp. 237–250.

[10] B. Hu, Y. Wang, and Z. Shi, "Simultaneous position and reflector estimation (SPRE) by single base-station," in *Proc. IEEE Wireless Commun. Netw. Conf. (WCNC)*, 2018, pp. 1–6.

[11] J. Talvitie *et al.*, "High-accuracy joint position and orientation estimation in sparse 5G mmWave channel," in *2019 IEEE Int. Conf. Commun. (ICC)*, 2019, pp. 1–7.

[12] Q. Bader, S. Saleh, M. Elhabiby, and A. Noureldin, "Leveraging single-bounce reflections and onboard motion sensors for enhanced 5G positioning," *IEEE Trans. Intell. Transp. Syst.*, vol. 25, no. 12, pp. 20 464–20 477, 2024.

[13] S. Parkvall *et al.*, "5G NR release 16: Start of the 5G evolution," *IEEE Commun. Stand. Mag.*, vol. 4, pp. 56–63, 2020.

[14] Y. Wang *et al.*, "Recent progress on 3GPP 5G positioning," in *Proc. IEEE 97th Veh. Technol. Conf. (VTC2023-Spring)*, 2023, pp. 1–6.

[15] S. Bauer, Y. Alkhorshid, and G. Wanielik, "Using high-definition maps for precise urban vehicle localization," in *Proc. IEEE 19th Int. Conf. Intell. Transp. Syst. (ITSC)*, 2016, pp. 492–497.

[16] Y. Ge *et al.*, "Exploiting diffuse multipath in 5G SLAM," in *Proc. IEEE Global Commun. Conf. (GLOBECOM)*, 2020, pp. 1–6.

[17] H. L. Van Trees, *Optimum Array Processing*. John Wiley & Sons, Ltd, 2002, ch. 7, pp. 710–916.

[18] H. Yi and X. Zhou, "On 2D forward-backward spatial smoothing for azimuth and elevation estimation of coherent signals," in *Proc. IEEE Antennas Propag. Soc. Int. Symp.*, vol. 2B, 2005, pp. 80–83.

[19] M. N. El korso, G. Bouleux, R. Boyer, and S. Marcos, "Sequential estimation of the range and the bearing using the zero-forcing music approach," in *Proc. 17th European Signal Process. Conf.*, 2009, pp. 1404–1408.

[20] M. Brambilla *et al.*, "Integration of 5G and GNSS technologies for enhanced positioning: An experimental study," *IEEE Open J. Commun. Soc.*, vol. 5, pp. 7197–7215, 2024.

[21] B. Camajori Tedeschini *et al.*, "A feasibility study of 5G positioning with current cellular network deployment," *Sci. Rep.*, vol. 13, no. 1, 2023.

[22] F. Gustafsson and F. Gunnarsson, "Mobile positioning using wireless networks: possibilities and fundamental limitations based on available wireless network measurements," *IEEE Signal Process. Mag.*, vol. 22, no. 4, pp. 41–53, 2005.

[23] European Telecommunications Standards Institute (ETSI), "Intelligent Transport Systems (ITS); vehicular communications; basic set of applications; part 2: Specification of cooperative awareness basic service," ETSI, Tech. Rep., 2014.